Variations of the Global Net Air–Sea Heat Flux during the "Hiatus" Period (2001–10)

XINFENG LIANG

College of Marine Science, University of South Florida, St. Petersburg, Florida

LISAN YU

Department of Physical Oceanography, Woods Hole Oceanographic Institution, Woods Hole, Massachusetts

(Manuscript received 2 September 2015, in final form 22 February 2016)

ABSTRACT

An assessment is made of the mean and variability of the net air–sea heat flux, Q_{net}, from four products (ECCO, OAFlux–CERES, ERA-Interim, and NCEP1) over the global ice-free ocean from January 2001 to December 2010. For the 10-yr "hiatus" period, all products agree on an overall net heat gain over the global ice-free ocean, but the magnitude varies from 1.7 to 9.5 W m^{-2}. The differences among products are particularly large in the Southern Ocean, where they cannot even agree on whether the region gains or loses heat on the annual mean basis. Decadal trends of Q_{net} differ significantly between products. ECCO and OAFlux–CERES show almost no trend, whereas ERA-Interim suggests a downward trend and NCEP1 shows an upward trend. Therefore, numerical simulations utilizing different surface flux forcing products will likely produce diverged trends of the ocean heat content during this period. The downward trend in ERA-Interim started from 2006, driven by a peculiar pattern change in the tropical regions. ECCO, which used ERA-Interim as initial surface forcings and is constrained by ocean dynamics and ocean observations, corrected the pattern. Among the four products, ECCO and OAFlux–CERES show great similarities in the examined spatial and temporal patterns. Given that the two estimates were obtained using different approaches and based on largely independent observations, these similarities are encouraging and instructive. It is more likely that the global net air–sea heat flux does not change much during the so-called hiatus period.

1. Introduction

Air–sea heat exchange directly links the ocean and the atmosphere and is an important factor for controlling the atmospheric and oceanic circulations (e.g., IPCC 2013). The net air–sea heat flux, Q_{net}, which includes radiative (shortwave and longwave) and turbulent (latent and sensible) components, displays temporal and spatial variations on a variety of scales, reflecting the complex interaction between the ocean and atmosphere (e.g., Yu and Weller 2007). Knowing how the net air–sea heat flux varies on different spatial and temporal scales is critically important for detecting and understanding the consequences of climate change and climate variability on the ocean heat budget and the ocean circulations (Trenberth et al. 2009).

On the interannual or longer time scales, a related and recently topical theme in the ocean and climate community is the "hiatus" of the global surface temperature increase since the beginning of the twenty-first century (e.g., Levitus et al. 2009; Meehl et al. 2011). Considering the existence of natural variability in the climate system, the change rate of the global surface temperature is not expected to be constant. This seeming hiatus of global warming, thus, is not that surprising for climate scientists. It nevertheless provides good motivation to investigate the climatic mechanisms working on the interannual and longer time scales. In the past years, a number of plausible explanations for the recent hiatus have been proposed, such as the change of the deep ocean heat uptake (e.g., Chen and Tung 2014), a reduced radiative forcing (e.g., Solomon et al. 2011), and even possible artifacts of data biases (e.g., Karl et al. 2015). It is natural to ask whether we can detect and understand the hiatus using time series of Q_{net}. If Q_{net} did not change, or if it even increased,

Corresponding author address: Xinfeng Liang, College of Marine Science, University of South Florida, 140 7th Avenue South, St. Petersburg, FL 33701.
E-mail: liang@usf.edu

DOI: 10.1175/JCLI-D-15-0626.1

during the hiatus period, the deep ocean heat uptake likely plays an important role in producing the hiatus. On the other hand, if Q_{net} decreased, both ocean dynamics and radiative forcing could contribute. Note that time series of the radiative and turbulent components of Q_{net}, if available and reliable, can help further understand the recent hiatus. For example, if the hiatus is due to a reduced radiative forcing (e.g., Solomon et al. 2011), the trend of the radiative fluxes should generally be consistent with that of the turbulent flux (Booth et al. 2012). However, if the hiatus is caused by long-period (interannual and longer) ocean variability (e.g., Chen and Tung 2014), the change of turbulent heat fluxes should be more significant (e.g., Gulev et al. 2013). A detailed analyses of those components are beyond the scope of this paper, and we will focus on their sum, the net air–sea heat flux, Q_{net}.

At present, a number of air–sea heat flux products are available. Based on the sources of measurements and approaches, the products can be grouped into atmosphere reanalysis, ocean syntheses, satellite and ship measurements–based products, and blended products that synthesize information from different sources (e.g., Josey et al. 2013). The spatially and temporally unevenly distributed samplings of in situ measurements, the near-surface air temperature and humidity that cannot be directly retrieved from satellites, the varying subgrid-scale parameterizations, and changes related to the observational systems introduce a great number of uncertainties into the estimates of Q_{net} (e.g., Yu et al. 2013). Because of the great differences in measurements and methodologies that are employed to produce these various Q_{net}, they can roughly be considered as quasi-independent estimates. Consistent features revealed in these products, which include largely independent uncertainties, can be viewed as robust and are likely more reliable. Moreover, examining the degree of consistency among them would shed useful light on the existing gap between different existing efforts and provide instructive implications for future works. A similar effort focusing on the ocean and coupled reanalyses over 1993–2009 was recently conducted by Valdivieso et al. (2016).

When integrated spatially and/or temporally, the uncertainty of the estimates of Q_{net} can accumulate and affect the physical representation of Q_{net}. The uncertainty of the global integrals of the existing Q_{net} products is far larger than $0.1\,W\,m^{-2}$, which is the accuracy required to address the human-induced energy imbalance (e.g., Wunsch and Heimbach 2014). Their variability on smaller spatial and shorter time scales is much larger. For instance, the 20-yr mean of the ECCO Q_{net} estimates shows basin-scale variability that is above $200\,W\,m^{-2}$; also, temporal variability in many regions, such as the major western boundary currents, is up to $200\,W\,m^{-2}$ as well (e.g., Liang et al. 2015). This implies that the Q_{net} response to climate change and climate variability could be strongly localized. Examination of the potentially robust spatial and temporal variability of Q_{net} during the so-called hiatus period could provide useful information for understanding the physics of air–sea heat exchange and the heat exchange between ocean basins.

In this study, we analyze the Q_{net} products from four representative efforts: an ocean state estimate from the Estimating the Circulation and Climate of the Ocean (ECCO) project (Wunsch and Heimbach 2013); the combination of the Objectively Analyzed Air–Sea Fluxes (OAFlux; Yu and Weller 2007) and the Clouds and the Earth's Radiant Energy System (CERES; Kato et al. 2013); a third-generation atmospheric reanalysis from the European Centre for Medium-Range Weather Forecasts interim reanalysis (ERA-Interim; Dee et al. 2011); and a first-generation atmospheric reanalysis from the National Centers for Environmental Prediction (NCEP) and National Center for Atmospheric Research (NCAR), NCEP1 (Kalnay et al. 1996). Annual and global means of the monthly values of Q_{net} during the overlapping 2001–10 from four representative products show significant differences in the long-term variation (Fig. 1). Although both ECCO and OAFlux–CERES do not show clear trends on the 10-yr time scale, ERA-Interim shows a decreasing trend and NCEP1 suggests an increasing one. So what trend, if any, is correct? And what are the reasons for these discrepancies among the four products? In this paper we attempt to address these questions.

The presentation is structured as follows. Section 2 provides a brief description of the four Q_{net} products and the interrelationships between them. Section 3 presents the intercomparison of the products, with special emphasis placed on the time mean and variability on interannual and longer time scales. Discussion and summary are presented in section 4. For people who are interested, the appendix provides a detailed intercomparison of the seasonal cycle of Q_{net} for the four products.

2. Description of products

The four products used in the study, ECCO, OAFlux–CERES, ERA-Interim, and NCEP1, represent the various efforts that have been made by ocean state estimation, satellite flux analysis, and atmospheric reanalysis communities to improve the

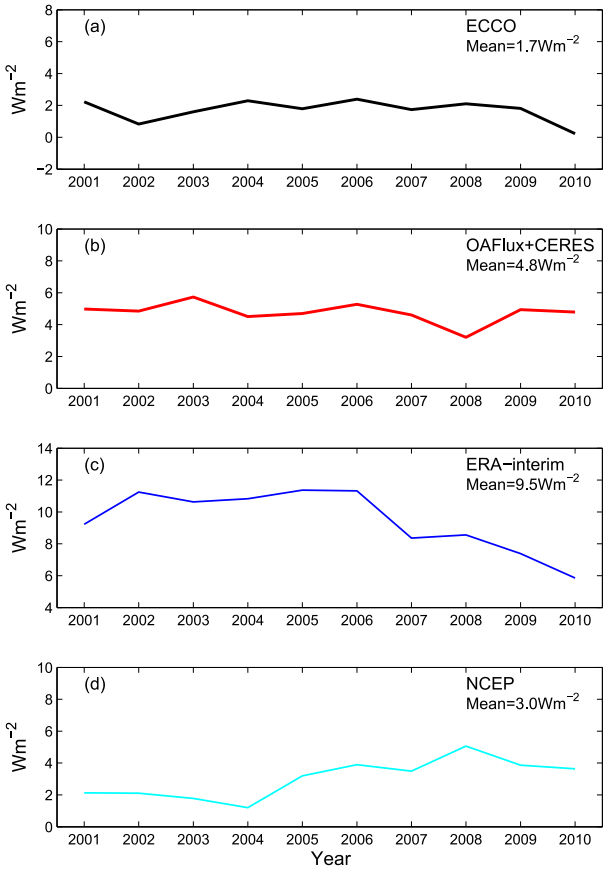

FIG. 1. Time series of the annual means of the global net air–sea heat flux from (a) ECCO, (b) OAFlux–CERES, (c) ERA-Interim, and (d) NCEP1. Positive (negative) values indicate the ocean receiving (losing) heat.

homogeneity and accuracy of long-term climate records. A brief description of the four products is provided below.

a. ECCO

ECCO is a state-of-the-art ocean state estimate (also known as ocean synthesis) and can be interpreted as a least squares fitting of an ocean general circulation model [the Massachusetts Institute of Technology General Circulation Model (MITgcm)] to the available global-scale ocean observations, such as sea level anomaly from altimeters and in situ temperature profiles from Argo. A major advantage of ECCO, compared with other oceanic and atmospheric reanalysis, is that the ECCO estimates satisfy known equations of motion and conservation laws, so no artificial internal sources and sinks are introduced into the estimates through the data assimilation (e.g., Wunsch and Heimbach, 2013). Also, the ECCO estimates can be directly used to understand how the ocean dynamics affects the air–sea fluxes.

A number of ECCO estimates are available. Stammer et al. (2004) presented the air–sea fluxes from an early version. In this present study, Q_{net} from the latest ECCO estimate (version 4, release 1) is analyzed. This estimate has 1° zonal resolution and a meridional resolution ranging from about 0.25° near the equator and poles to 1° at midlatitudes. It covers the period from 1992 to 2011. A priori forcing fields are from the ERA-Interim reanalysis (Dee et al. 2011). Surface atmospheric states (temperature, humidity, downward radiation, precipitation, and wind stress) are control parameters and are adjusted through the adjoint. Latent, sensible, and upward radiative components of Q_{net} are computed using the bulk formulas of Large and Yeager (2004) and the adjusted near-surface atmospheric states. See Wunsch and Heimbach (2013) and Forget et al. (2015) for more information.

b. OAFlux–CERES

The OAFlux turbulent air–sea latent and sensible heat fluxes (Yu and Weller 2007; Yu et al. 2008) and the CERES Energy Balanced and Filled (EBAF) surface radiation products (Kato et al. 2013) are the leading products among the efforts that construct global air–sea fluxes from satellite observations of surface and atmospheric state variables. The combination of the two has the potential to produce one of the best available estimates for the net air–sea heat flux.

The OAFlux latent and sensible heat flux products were constructed from bulk flux parameterization using input air–sea variables (i.e., wind speed, air humidity, air temperature, and sea surface temperature) estimated from objective synthesis (Yu et al. 2008). The objective synthesis was based on a least squares estimator that seeks the optimal values for the flux-related variables that best fit input data sources. The version used here is the new 0.25° gridded analysis that has been recently developed using satellite observations from 1987 to present (Yu and Jin 2014a,b; Jin et al. 2015). Different from the previous 1° version, no reanalysis products are used in this new analysis. OAFlux used buoy time series measurements at 100+ locations for evaluation (Yu et al. 2007). The buoy evaluation shows that the OAFlux latent and sensible heat flux estimates have a mean difference (or bias) of 1.6 W m^{-2} and a root-mean-square (rms) difference of 9.6 W m^{-2}.

The CERES EBAF surface radiative fluxes were derived from the CERES SYN1deg-Month Ed3 (e.g., Loeb et al. 2009; Kato et al. 2013). The CERES fluxes are delivered on monthly 1° × 1° grids starting from March 2001. A comparison with surface buoy observations shows that the mean (rms) difference between CERES and buoys is 4.7 (13.3) W m^{-2} for downward

shortwave and −2.5 (7.1) W m^{-2} for downward longwave radiation over the oceans (Kato et al. 2013).

c. NCEP1 and ERA-Interim

NCEP1 is a first-generation global reanalysis of atmospheric data spanning 1948 to present that is available as a global set of gridded data at a 2.5° × 2.5° horizontal resolution (Kalnay et al. 1996). ERA-Interim is the latest global atmospheric reanalysis produced by ECMWF that covers the period from 1979 onward at 80 km (~0.7°) spatial resolution (Dee et al. 2011). Atmospheric reanalysis uses numerical weather prediction (NWP) models to assimilate a significant amount of observational data. The atmospheric reanalysis usually does not include ocean models, so the ocean's influence and response are mainly represented by the chosen boundary condition (i.e., the sea surface temperature). Also, because of the forecasting nature of atmospheric reanalysis, observations are assimilated sequentially and adjustments are usually made within short-range assimilation windows. For instance, the NCEP1 data assimilation system is a 6-hourly three-dimensional variational analysis (3DVar), while the ERA-Interim includes a four-dimensional variational analysis (4DVar) with a 12-h analysis window. These data assimilation systems are different from the nonsequential method in ECCO and the atmospheric reanalysis does not evolve fully satisfying the model equations. It thus includes artificial jumps, making assessment of the long-term variation of Q_{net} challenging.

d. Relationships among products

Although the four Q_{net} products are produced at five different centers, they are not entirely independent. The a priori forcing fields of ECCO are from ERA-Interim. Thus Q_{net} from ECCO can be roughly interpreted as an adjusted estimate of ERA-Interim, constrained by ocean observations and dynamics. The OAFlux–CERES Q_{net} values are obtained from satellite observations using no dynamical models but the state-of-the-art flux algorithms and statistical approaches. In addition, OAFlux–CERES makes use of observations from meteorological satellites, whereas ECCO assimilates oceanic observations from a variety of sources, such as oceanographic satellites and Argo profiles. OAFlux and CERES share no common observational resources with ECCO, except SST (Reynolds SST). The Q_{net} estimates from atmospheric reanalysis strongly depend on the numerical models and parameterizations that are utilized in the systems. The quality, quantity, and types of observations that are assimilated also play an important role in generating the final estimates. NCEP1 and ERA-Interim are different in a number of ways, such as numerical models and boundary conditions (i.e., SST). In summary, although the four products are not entirely independent, they are different in so many ways that they can be considered as quasi-independent.

The study period is focused on the 10 years from January 2001 to December 2010, the period that a full record of Q_{net} can be obtained from all sources. Monthly-mean global fields are used, which allow an examination of the Q_{net} mean and variability on seasonal, interannual, and longer time scales. Because of the low temporal resolution of the four products, high-frequency components are not quantified. Before conducting the analysis, we interpolated all of the original estimates to global grids of 1° × 1° and then applied the same ocean and ice masks to the interpolated values to focus on the ice-free ocean. The use of a sea ice mask is based on the consideration that the satellite-based OAFlux product does not provide flux estimates within 50 km of the coast or the ice edge due to the lack of reliable retrievals. The ice mask was derived from the National Snow and Ice Data Center (NSIDC) based on the 50% sea ice concentration threshold (Yu et al. 2008).

3. Analysis

a. The time mean fields

The global and 10-yr averages of Q_{net} from ECCO, OAFlux–CERES, ERA-Interim, and NCEP1 over the ice-free ocean are 1.7, 4.8, 9.5, and 3.0 W m^{-2}, respectively. All imply that the ocean received heat during the period 2001–10 but the magnitude of the heat gain varies with product. The 10-yr means of the net air–sea heat flux, $\overline{Q_{net}}$, from the four products over the global ice-free ocean show both similarities and discrepancies (Fig. 2). The similarities are characterized by three aspects. First, all products show the well-known spatial pattern of $\overline{Q_{net}}$ over the global ocean; that is, the ocean receives heat in the tropics and loses it at higher latitudes. Second, intense air–sea heat exchange generally occurs in the vicinity of ocean frontal regions (e.g., the cold tongues in the eastern equatorial Pacific and Atlantic), the warm western boundary currents (e.g., the Gulf Stream and the Kuroshio), and the high-latitude North Atlantic. The largest magnitude of $\overline{Q_{net}}$ is about 200 W m^{-2}. Third, the eastern boundary upwelling systems are associated with strong air–sea heat exchange, indicating the impacts of ocean upwelling on the air–sea heat exchange.

Discrepancies between the four $\overline{Q_{net}}$ are most evident in the Southern Ocean, where ECCO and OAFlux–CERES display limited regions of positive values but ERA-Interim and NCEP1 show a dominance of positive

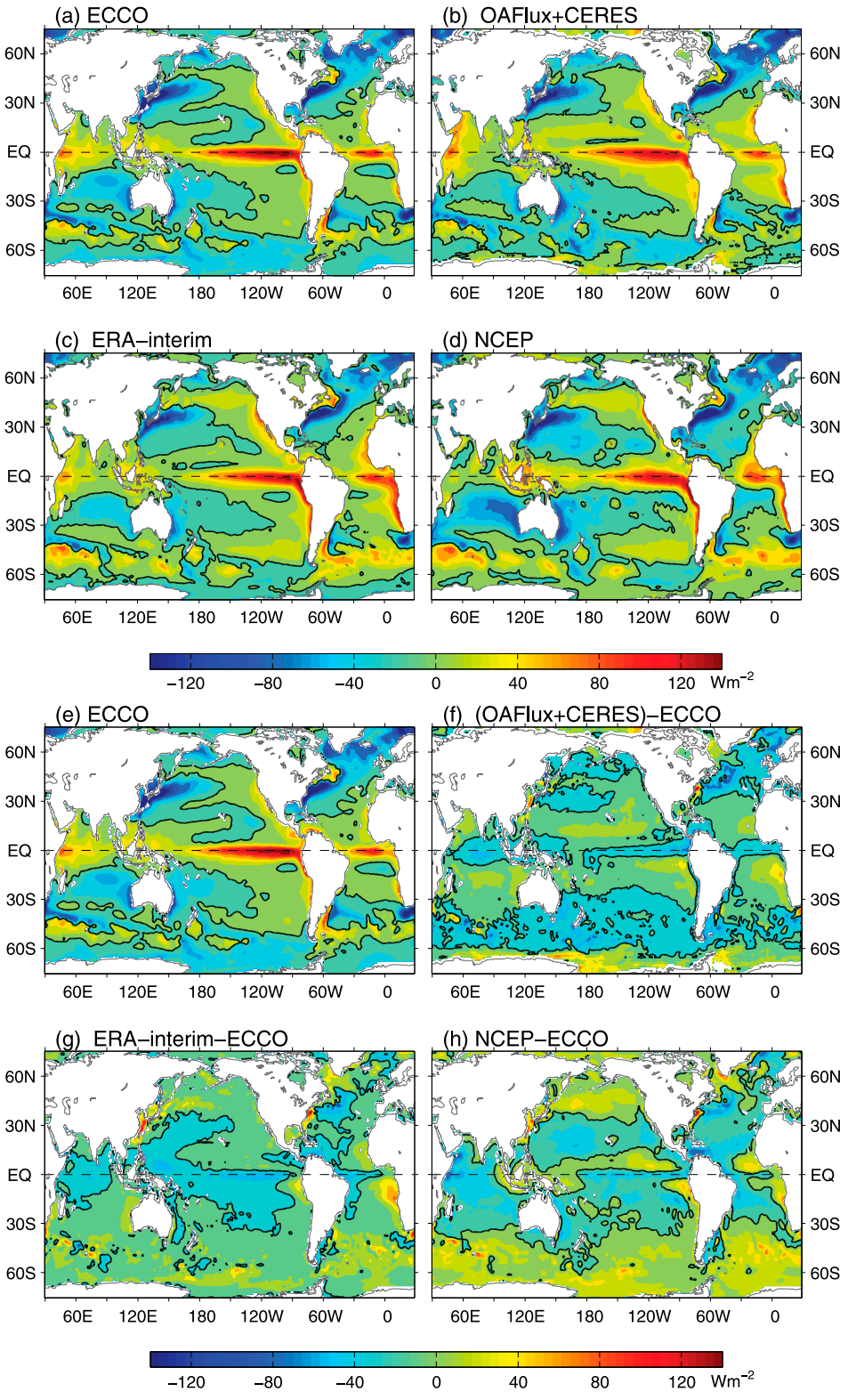

FIG. 2. (top) 10-yr means of Q_{net} from (a) ECCO, (b) OAFlux–CERES, (c) ERA-Interim, and (d) NCEP1. Zero contours are marked in black. Positive (negative) values indicate ocean receiving (losing) heat. (bottom) 10-yr mean of Q_{net} from (e) ECCO and the differences of (f) OAFlux–CERES, (g) ERA-Interim, and (h) NCEP1 from ECCO.

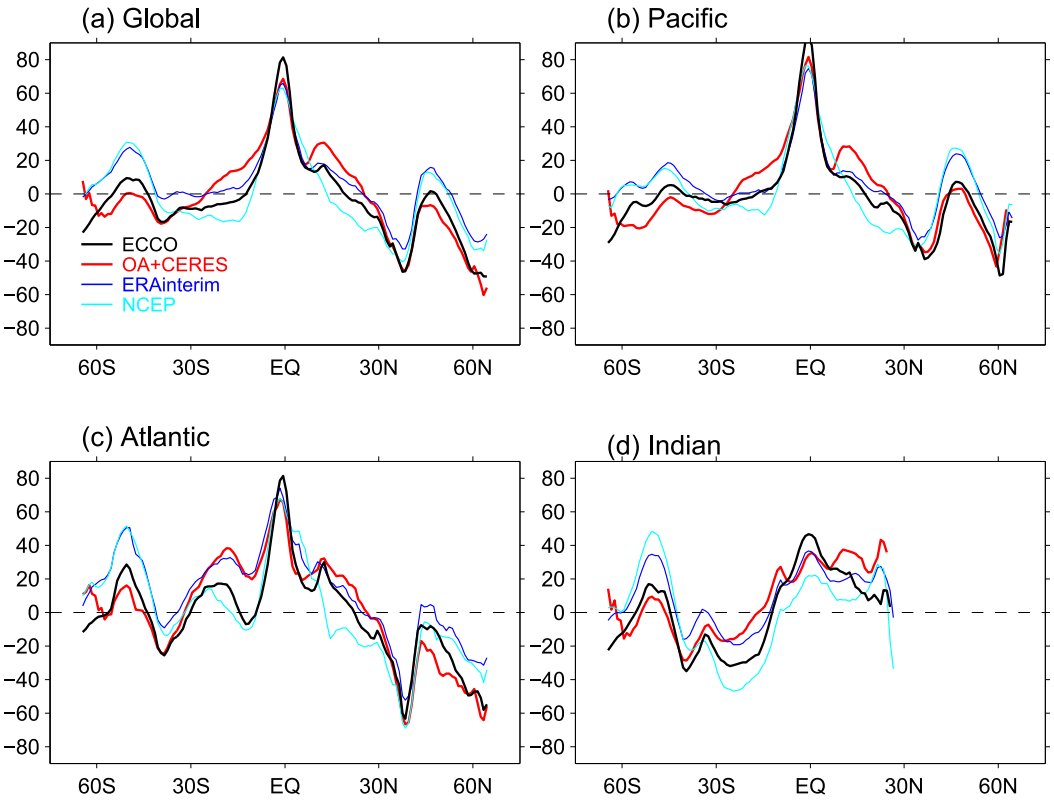

FIG. 3. Zonal averages of the 10-yr means of Q_{net} for (a) the global ocean, (b) the Pacific, (c) the Atlantic, and (d) the Indian Ocean. Positive (negative) values stand for ocean receiving (losing) heat.

values (Figs. 2 and 3a). In other words, the four products do not agree on whether the Southern Ocean, a region of high climate sensitivity (e.g., Bourassa et al. 2013), received or lost heat between 2001 and 2010. As suggested in several previous studies (e.g., Bromwich and Fogt 2004), a lack of sufficient observations at high southern latitudes is likely the reason for the disagreement. Recall the fact that the ECCO estimates were adjusted from ERA-Interim, the similarity between ECCO and OAFlux–CERES suggests they may better represent the time-mean air–sea heat exchange, particularly at higher latitudes.

Zonal averages of $\overline{Q_{net}}$ are constructed for the global ocean and three major basins: the Pacific, Indian, and Atlantic Ocean basins (Fig. 3). The zonal patterns summarize the main features identified in Fig. 2. Despite the difference in magnitude, all products show similar latitudinal variations on both global and basin scales. For example, all products show maxima centered at the equator and around 50°N/S. In addition, the values of the zonally averaged $\overline{Q_{net}}$ are consistent near the equator in both the global and the basinwide averages, suggesting a convergence of the products in presenting the 10-yr mean net heat exchange in the tropical region.

The discrepancy in the globally zonal averaged $\overline{Q_{net}}$ occurs primarily at middle and high latitudes (Fig. 3a). The global zonal averages differ by about 20 W m^{-2} north of 45°N and about 30 W m^{-2} in the north and south subtropical oceans as well as in the Southern Ocean poleward of 40°S. In some regions, even the signs of the zonally averaged $\overline{Q_{net}}$ differ between products. For instance, both OAFlux–CERES and ECCO have an ocean heat loss in the Northern Hemisphere around 50°N, but NCEP1 and ERA-Interim show ocean heat gain (Fig. 3a). In general, OAFlux–CERES and ECCO show a better consistency with each other at higher latitudes, while NCEP1 and ERA-Interim have a good agreement between themselves. The zonally averaged $\overline{Q_{net}}$ were also constructed for the Pacific (Fig. 2b), Atlantic (Fig. 2c), and Indian (Fig. 2d) Oceans, all showing significant discrepancies in magnitude. Large discrepancies will therefore be expected in meridional ocean heat transports that are inferred from the meridional convergence of the Q_{net} products.

b. *Variability on interannual and longer time scales*

If seasonal cycles are removed, the standard deviations of the monthly Q_{net} anomalies, σ_{ia}, can be used

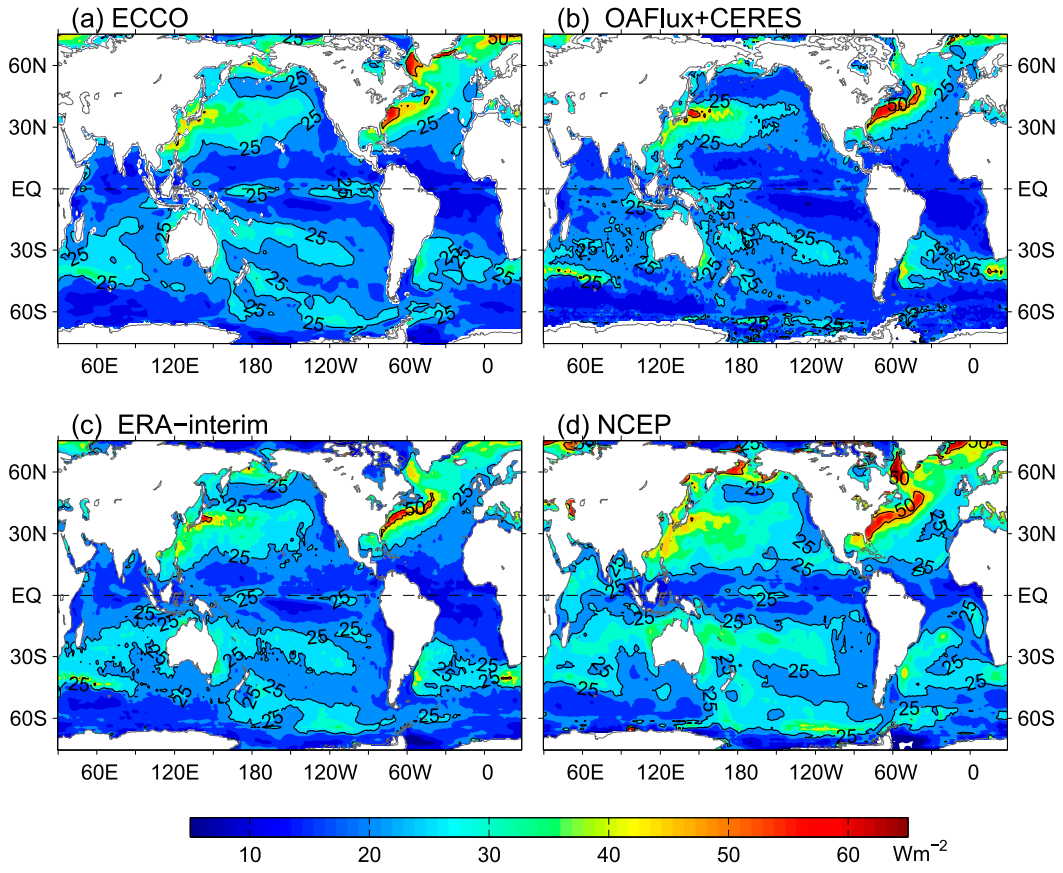

FIG. 4. Standard deviation of monthly Q_{net} anomalies from (a) ECCO, (b) OAFlux–CERES, (c) ERA-Interim, and (d) NCEP. The contour interval is 50 W m^{-2} (seasonal cycle removed).

to characterize the Q_{net} variability on interannual and longer time scales. For people who are interested, the appendix provides a detailed intercomparison of the seasonal cycle of Q_{net} for the four products. Since only seasonal cycles were removed from the original time series, some high-frequency components, such as the intraseasonal variability, were left in the monthly Q_{net} anomalies. Because of the low temporal resolution (monthly) of the four products, those high-frequency components are hard to quantify here. In this study, we simply assume that averaging over a year will significantly reduce the impact of those high-frequency components.

In general, the magnitude of lower-frequency variability of Q_{net} is smaller than that of the seasonal cycles (Figs. 4 and A1). In all products, the patches of large σ_{ia} (>25 W m^{-2}) are shown in the western boundary currents, implying an important role of the ocean circulation in the low-frequency variations of the air–sea heat exchange. Large σ_{ia} (>25 W m^{-2}) also appears in the subpolar North Atlantic, which could be related to the North Atlantic Deep Water (NADW) production/deep convection. In the Southern Hemisphere, bands of large σ_{ia} (e.g., the band around 30°S in the Pacific) are observed in all products, although the spatial extent of those bands varies with products. Globally, the tropical ocean, except right at the equator, is the region of weak low-frequency variability (<20 W m^{-2}).

A detailed intercomparison of the spatial structure of σ_{ia} reveals a number of disagreements among the four products (Fig. 4). NCEP1 has the least agreement with the three other products, showing strong low-frequency variability (>25 W m^{-2}) in a major portion of the global ocean. NCEP1 differs also from other products in the equatorial region, where the low-frequency variability of Q_{net} is closely related to El Niño–Southern Oscillation (ENSO). Specifically, ECCO, OAFlux–CERES, and ERA-Interim show larger σ_{ia} in the eastern and western tropical Pacific, but NCEP1 only shows a small intense patch in the middle of the tropical Pacific. The deviation of NCEP1 from the other three products is also evidenced in the tropical Indian Ocean, where the low-frequency variability from NCEP1 is significantly larger.

Monthly evolution of the zonally averaged Q_{net} anomalies (seasonal cycle removed) is shown in Fig. 5.

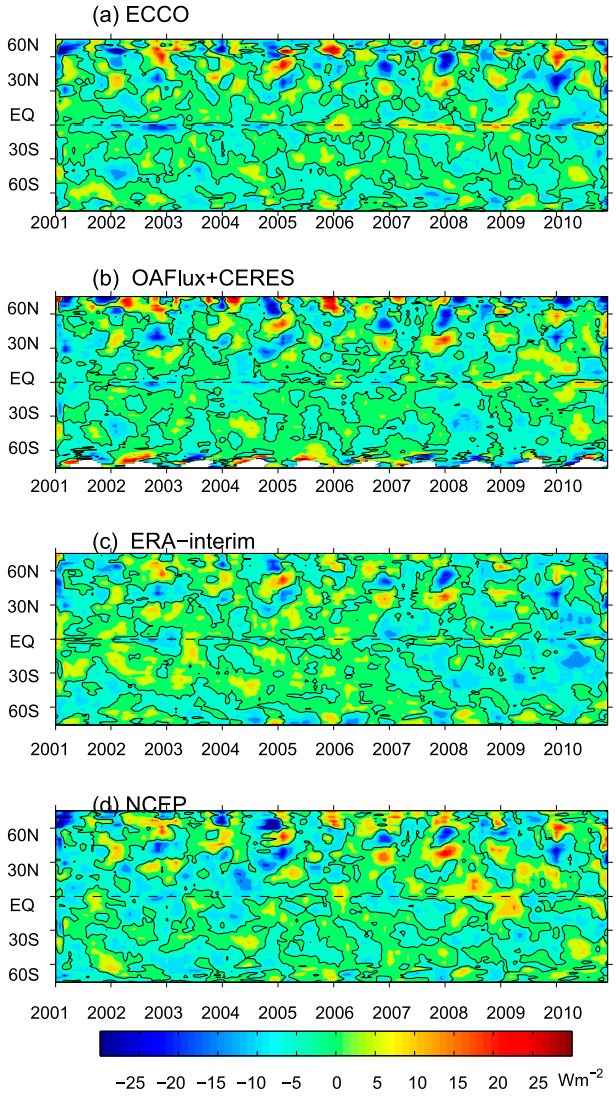

FIG. 5. Temporal evolution of the zonally averaged Q_{net} anomalies from (a) ECCO, (b) OAFlux–CERES, (c) ERA-Interim, and (d) NCEP. The contour interval is 50 W m^{-2} (seasonal cycle removed).

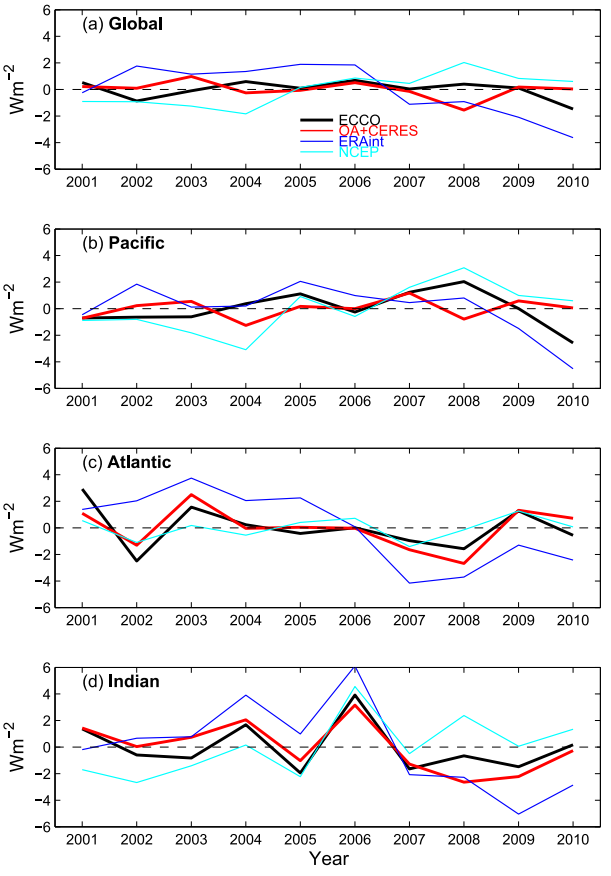

FIG. 6. Time series of monthly Q_{net} anomalies, global and basin averages. Seasonal cycle is removed. Note the encouraging similarity between ECCO and OAFlux–CERES.

While the pattern is generally noisy, there are consistent features across all the products. For instance, large temporal variations appear at high latitudes of the Northern Hemisphere. The most notable discrepancy is in the evolution of the pattern with time. ERA-Interim shows that Q_{net} anomalies changed from mostly positive to mostly negative around 2006/07. NCEP1 Q_{net} anomalies also experienced a pattern change but with an opposite sign, from mostly negative to mostly positive around 2005/06. By comparison, ECCO and OAFlux–CERES have no clear pattern change during the 10-yr period. Further examination suggests that these pattern differences mainly appear within the latitudinal range 30°N–30°S. The discrepancy of the low-frequency variability of Q_{net} in the tropical and subtropical regions is a plausible cause for the different long-term trends in the four products (see Fig. 1).

Annual and global means of the monthly Q_{net} anomalies for the four products differ from each other, not only in magnitude but also in temporal pattern (Fig. 6a). The large spread suggests a large uncertainty within the four products in depicting the long-term variation of the global integrals of Q_{net}. The mean of the spread (the largest difference among all products) is about 3.6 W m^{-2}, far exceeding the needed accuracy (~0.1 W m^{-2}) for detecting the impact of the anthropogenic warming on the ocean heat content. On the global scale, it is therefore not possible using the four products to address the human-induced ocean warming directly while might still be usable for studying strong natural variabilities. We also calculated the monthly Q_{net} anomaly averages for the three major basins (Figs. 6b–d). The means of the spreads for the Pacific, Atlantic, and Indian Oceans are 3.9, 4.2, and 5.2 W m^{-2},

respectively. These large spreads suggest that, similar to the global scale, the low-frequency trend of Q_{net} on the basin scales should be interpreted with caution. Inferences, such as about the change of heat exchange between ocean basins, will greatly depend on the products that are utilized.

Decadal trends of the global- and basin-scale averages of Q_{net} were calculated by least squares fitting (Table 1). Great discrepancies exist among the four products on both the global and basin scales. In all cases, the four products do not even agree on the signs of the trends. For instance, on the global scale, ECCO and ERA-Interim show negative trends, but OAFlux–CERES and NCEP1 show positive trends. Note that although the signs of the trends for ECCO ($-0.5\,W\,m^{-2}\,decade^{-1}$) and OAFlux–CERES ($1.0\,W\,m^{-2}\,decade^{-1}$) are opposite, their magnitudes are significantly smaller than those for ERA-Interim ($-5.2\,W\,m^{-2}\,decade^{-1}$) and NCEP1 ($2.9\,W\,m^{-2}\,decade^{-1}$). Thus, the decadal change of the global averages of Q_{net} is notably smaller in ECCO and OAFlux–CERES than in ERA-Interim and NCEP1. On the basin scales, the consistency among the products is not better than on the global scale. In the Pacific, ERA-Interim shows a negative trend ($-3.1\,W\,m^{-2}\,decade^{-1}$), while the other three display positive trends (0.1–$3.7\,W\,m^{-2}\,decade^{-1}$). In the Indian Ocean, NCEP1 is the exception, presenting a large positive decadal trend ($4.4\,W\,m^{-2}\,decade^{-1}$), whereas the others show negative trends (-1.1 to $-5.3\,W\,m^{-2}\,decade^{-1}$). Even on the basin scale, we are not entirely sure how the air–sea heat flux changes on the decadal scale. An interesting observation that should be noted is that the decadal trends calculated from ECCO estimates are usually between those from the ERA-Interim and OAFlux–CERES products. The implication of this observation will be discussed below.

Despite the discrepancies among the four products, the low-frequency variability of ECCO Q_{net} is much more similar to OAFlux–CERES than to either ERA-Interim or NCEP1 during the ''hiatus'' period. An EOF analysis for the monthly Q_{net} anomalies within the region between 30°S and 30°N shows that the first two EOFs and the associated PCs for ECCO and OAFlux–CERES are almost identical. These two products show a striking similarity in both the spatial patterns of the EOFs and the temporal patterns of the PCs. As we mentioned above, ECCO estimates of Q_{net} can be considered as adjusted ERA-Interim Q_{net}. Thus, the departure of ECCO from ERA-Interim represents the adjustment that is constrained by ocean dynamics and ocean observations. The difference between ECCO and ERA-Interim suggests that the ERA-Interim pattern shift in 2006/07 (see Figs. 5 and 6) is not consistent with the ocean dynamics and observations. A similar observation about the suspicious pattern shift in ERA-Interim around 2006/07 was made in Chiodo and Haimberger (2010). They concluded that it comes mainly from the surface radiation flux time series, which could be due to the introduction of new satellite measurements around that time. The OAFlux–CERES Q_{net} values were obtained from satellite observations using no dynamical models but the state-of-the-art flux algorithms and statistical approaches. In addition, OAFlux–CERES make use of observations from meteorological satellites, whereas ECCO assimilates observations from oceanographic satellites and Argo profiles. The two products share no common observational resources except SST (both used the Reynolds SST). Furthermore, OAFlux and CERES are two independent groups, with each producing the best flux analysis in its respective field. Given the dissimilarity in the approaches used in estimating Q_{net}, the similarity in the low-frequency variability of Q_{net} between ECCO and OAFlux–CERES is revealing. It suggests that the low-frequency variability of the OAFlux–CERES Q_{net} has a sufficient accuracy to meet the requirement of dynamical consistency imposed by ocean state estimate, and that the pattern of decadal change delineated by the two Q_{net} products, an almost flat trend, may be a realistic representation of the air–sea heat flux during the hiatus period.

TABLE 1. Decadal trends of the global and basinwide averages of Q_{net} for ECCO, OAFlux–CERES, ERA-Interim, and NCEP1. The unit is $W\,m^{-2}\,decade^{-1}$.

Trends	Global	Pacific	Atlantic	Indian
ECCO	−0.5	0.1	−1.3	−1.1
OAFlux–CERES	1.0	2.1	0.5	−1.5
ERA-Interim	−5.2	−3.1	−6.8	−5.3
NCEP1	2.9	3.7	0.6	4.4

Figure 5 shows that the discrepancy of the low-frequency variability of Q_{net} among the four products largely occurs in the tropical region (30°S–30°N). Here we briefly investigate the causes of this disparity by focusing on Q_{net} in the tropical region. The monthly evolution of Q_{net} anomalies averaged between 30°S and 30°N is displayed in Fig. 7. Despite the differences in the detailed structures, ENSO-like variability is presented in all products. For instance, the ocean gained more heat from the atmosphere (positive anomalies) in the central and eastern equatorial Pacific during the cold event in 2008/09 and released more heat to the atmosphere (negative anomalies) during the warm events in 2002/03 and 2009/10. As shown in Mayer et al. (2013), the positive correlation between Q_{net} and SST implies an

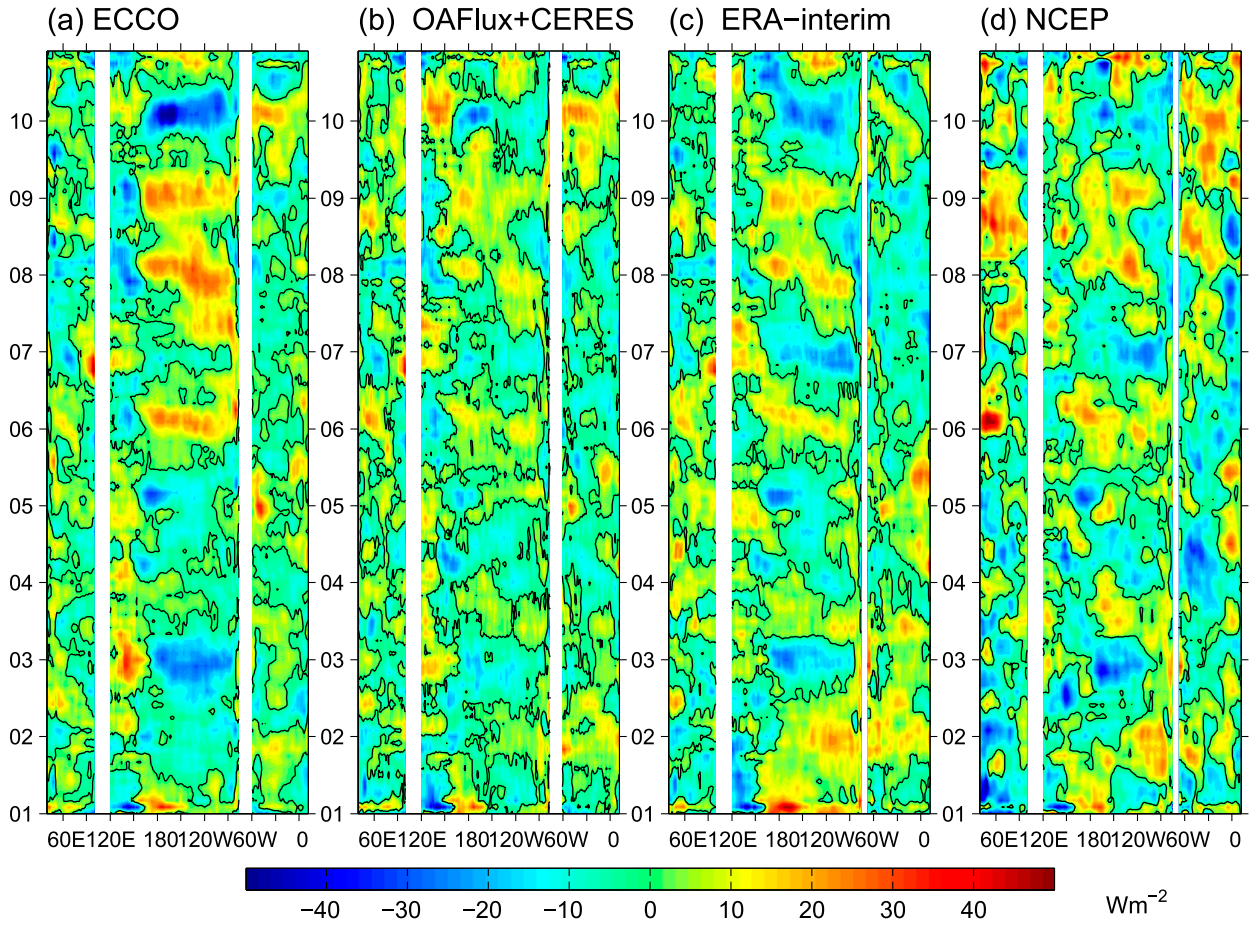

FIG. 7. Temporal evolution of the monthly Q_{net} anomalies averaged between 30°N and 30°S from (a) ECCO, (b) OAFlux–CERES, (c) ERA-Interim, and (d) NCEP. Positive (negative) values stand for ocean receiving (losing) heat.

atmospheric response to the ENSO SST. The differences of the four products in representing the tropical ocean dynamics could be the major cause of the disparity in the low-frequency Q_{net}. Furthermore, the variance of the Q_{net} anomalies is clearly larger in ECCO than in the other products, suggesting a stronger SST–flux feedback. In the Indian Ocean, ECCO, OAFlux–CERES, and ERA-Interim present a similar pattern, but NCEP1 displays significant differences, particularly after 2006. In the Atlantic Ocean, ECCO and OAFlux–CERES bear strong similarity to each other but differ from both NCEP1 and ERA-Interim.

4. Summary and discussion

This study presents a number of consistencies and discrepancies among four representative air–sea heat flux estimates from ECCO, OAFlux–CERES, ERA-Interim, and NCEP1 on the time mean, as well as interannual and longer time scales, over 2001–10. Following the time scales, the main results are summarized as follows:

1) The four products agree that the global ice-free ocean received heat between 2001 and 2010 but differ in the magnitude, ranging from 1.7 W m^{-2} (ECCO) to 9.5 W m^{-2} (ERA-Interim). During the period 2001–10, all products agree that the global ocean received heat in the tropical regions and lost it at higher latitudes, in the western boundary currents and in the North Atlantic. The spatial patterns of 10-yr means of Q_{net} show particularly bad agreement in the Southern Ocean. Whether the Southern Ocean received or lost heat between 2001 and 2010 is unclear.
2) All products show the largest variability on the interannual and longer time scales in the western boundary currents and the high latitudes of the North Atlantic. Although it remains challenging to detect the long-term trend of the global averages of Q_{net}, the similarity between ECCO and OAFlux–CERES

is encouraging. It suggests that the pattern of decadal change delineated by ECCO and OAFlux–CERES, almost no trend, may be a realistic representation of the air–sea heat exchange during the ''hiatus'' period. In contrast to the time-mean values, the largest uncertainty of the low-frequency variability of Q_{net} appears in the tropical regions (30°S–30°N), which results in the discrepancy in the long-term trends of Q_{net} (Fig. 1).

A few key regions for the air–sea heat exchange are revealed in this study. First, all products show that the western boundary currents are important on all the examined time scales. To accurately simulate the heat exchange between the ocean and the atmosphere, the western boundary currents should be represented correctly in the coupled atmosphere and ocean models. Second, the high-latitude regions, particularly the North Atlantic and the Southern Ocean, are also crucial regions on all the examined time scales. However, because of the lack of sufficient observations, huge uncertainties exist. As mentioned above, whether the Southern Ocean received or lost heat during the period 2001–10 remains unclear. More observations are therefore needed to reduce the uncertainties and improve the current estimates at higher latitudes. This is also discussed in detail in Bourassa et al. (2013). Third, although the tropical regions do not show strong seasonal cycles, they are the major locations where the heat enters the global ocean and are therefore crucial for the long time means of air–sea heat exchange. Fourth, the region in the vicinity of the equator, particularly in the Pacific Ocean, is important for the interannual variability of Q_{net}. This could be related to the tropical ocean dynamics, particularly ENSO. Finally, the eastern boundary upwelling systems are associated with strong time-mean air–sea heat exchange but do not appear particularly important on the seasonal and interannual time scales.

Consistency does not represent the accuracy of the products but provides useful implications for the data quality. In general, NCEP1 shows the most disagreement from the other three products on almost all of the examined time scales. Here, we thus focus on the relationships among ECCO, OAFlux–CERES, and ERA-Interim. First of all, ECCO and OAFlux–CERES show many similarities in the spatial patterns on different examined time scales, particularly in the long-term trend (Fig. 1) and the dominant EOF modes in the tropical regions. Because these two products are obtained using different approaches and based on largely non-overlapping observations, those similarities are encouraging. Second, ECCO used ERA-Interim to provide a priori forcing fields. As expected, ECCO and ERA-Interim display many similar features. However, ECCO also shows interesting differences from ERA-Interim, which are due to the constraints of the ocean observations and ocean dynamics. Third, the similarities of ECCO to OAFlux–CERES and its differences from ERA-Interim suggest that the ocean dynamics and ocean observations move ECCO away from ERA-Interim and close to OAFlux–CERES. Because CERES includes estimates of the heat flux at the top of the atmosphere and ECCO includes estimates of the ocean state, the similarity between these two products at the sea surface imply that we can combine ECCO, OAFlux, and CERES to understand the heat transport in the whole air–sea coupled system, from the top of the atmosphere to the bottom of the ocean.

Further studies are needed to understand the reasons for the discrepancies revealed above and to reduce the uncertainties of the currently existing products. First of all, a major reason for the uncertainty of the products is the lack of enough in situ observations, particularly at high latitudes (e.g., the Southern Ocean). This problem is more pronounced for the long-term mean and the seasonal cycles (see the appendix). With more in situ measurements, we can at least evaluate the existing products with much more confidence. Second, for the interannual and longer time scales, the key region is the tropics, where much more data are available than at the high latitudes but the dynamics are unique. A better way to assimilate the existing tropical observations to correctly represent the tropical dynamics seems to be a priority for the reanalysis products. It should be noted that a detailed examination of the possible reasons for these discrepancies requires dedicated efforts from all the groups that produce the existing products and is too ambitious to be addressed in this paper.

In summary, while all products agree that the globe ocean received heat over the so-called hiatus period, they differ significantly in the decadal trends of Q_{net}. Among the four products, ECCO and OAFlux–CERES produced almost no decadal trend for the global averages of Q_{net} (see Table 1). This similarity is encouraging, suggesting it is more likely that the global net air–sea heat flux does not change much during the hiatus period. Moreover, even on the ocean basin scales, all products do not show much consistency, suggesting that caution should be exercised in using these products to examine the basin-scale heat content changes, as well as the possible dynamical mechanisms, particularly in the context of anthropogenic impacts. Note that numerical simulations utilizing different surface heat flux products likely generate results showing distinct long-term trends. Discussion of the ocean heat content changes from numerical simulations should take into account the impact

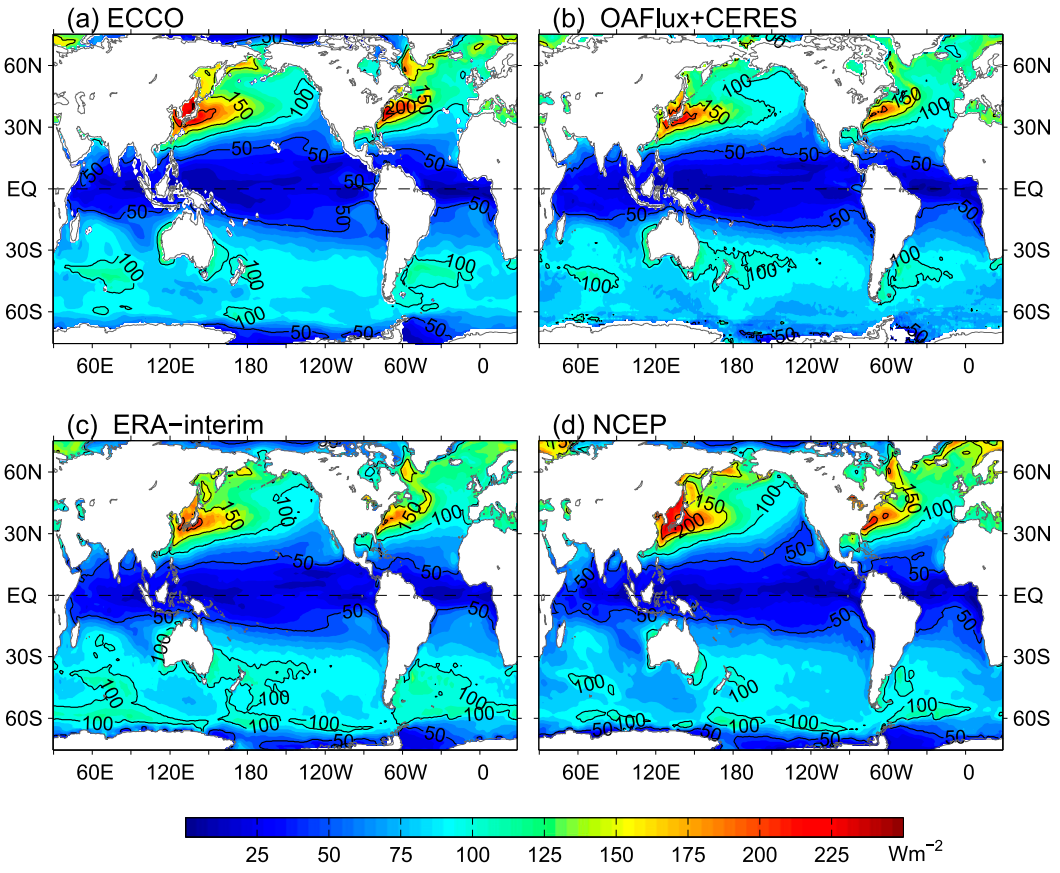

FIG. A1. Standard deviation of climatological monthly Q_{net} from (a) ECCO, (b) OAFlux–CERES, (c) ERA-Interim, and (d) NCEP. The contour interval is 50 W m^{-2}.

of the uncertainty of the existing air–sea heat flux products.

Acknowledgments. This paper is funded in part by the NOAA Climate Observation Division, Climate Program Office, under Grant NA09OAR4320129 and by the NOAA MAPP Climate Reanalysis Task Force Team under Grant NA13OAR4310106. The study was initiated when X. Liang was a postdoc at MIT, where he was supported in part by the NSF through Grant OCE-0961713, by NOAA through Grant NA10OAR4310135, and by the NASA Physical Oceanography Program through ECCO. We thank Carl Wunsch, Patrick Heimbach, and Rui Ponte for their helpful comments on an early version of this manuscript. We appreciate Xiangze Jin's effort in making the 0.25-degree OAFlux analysis available. The ERA-Interim and NCEP1 reanalyses were downloaded from the NCAR Research Data Archive (http://rda.ucar.edu). OAFlux products are available from the project website (http://oaflux.whoi.edu/). CERES and ECCO products were downloaded from their websites (http://ceres.larc.nasa.gov; http://www.ecco-group.org).

APPENDIX

The Seasonal Cycle of Q_{net}

To examine the seasonal cycle of Q_{net}, we first calculated the climatological monthly data over the period 2001–10. The standard deviation, σ_s, of the 12 climatological monthly Q_{net} values is constructed to delineate the seasonal variability in the four products (Fig. A1). The products agree well in the general spatial pattern, with relatively weak ($\sigma_s < 50\,\mathrm{W\,m^{-2}}$) seasonal variations in the tropical region and strong ($\sigma_s > 100\,\mathrm{W\,m^{-2}}$) seasonal variations in the western boundary currents and at higher latitudes. The largest σ_s values (>200 W m^{-2}) are associated with the Gulf Stream and the Kuroshio, indicating the role of the western boundary currents in influencing the regional air–sea heat exchange processes. On the other hand, the products are different in the detailed spatial structures, particularly at higher southern latitudes. South of 45°S, the regions with large σ_s (>100 W m^{-2}) are much more extended in ERA-Interim than in the other products.

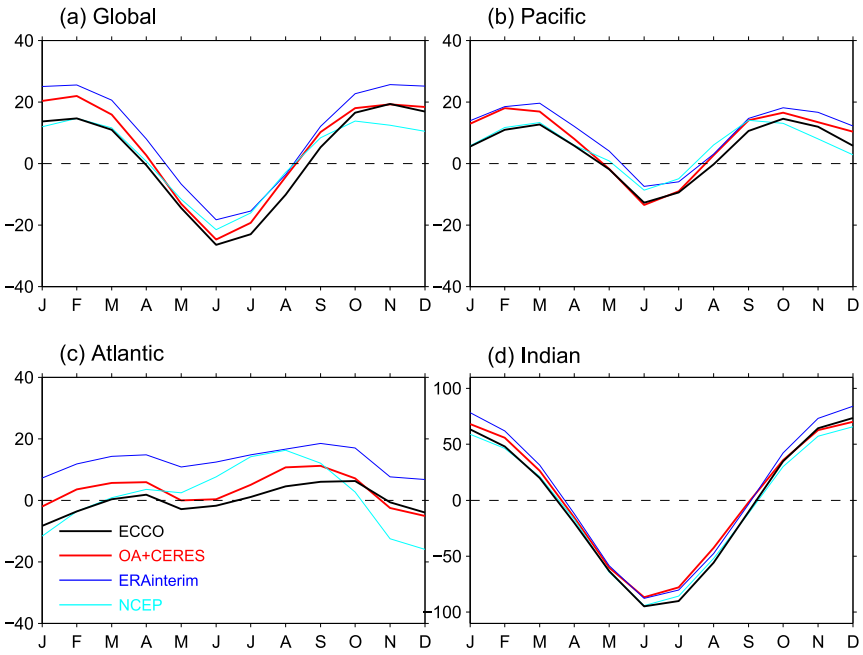

FIG. A2. Seasonal cycle of Q_{net} averaged over the globe and three major ocean basins.

Figure A2 displays the seasonal cycle of Q_{net} averaged over the globe and three major ocean basins. There is a good agreement in the temporal patterns of the seasonal cycles except for the Atlantic Ocean. Globally, the ocean loses heat to the atmosphere between April and August, while it gains heat from the atmosphere between August and March. In other words, there is a net ocean warming in the boreal winter and a net cooling in the boreal summer. ERA-Interim has the largest Q_{net} throughout the seasonal cycle, and its cooling season—which starts in May, about one month later than the three other products—is also the shortest. The seasonal cycle of ECCO is in phase with ERA-Interim, but the overall magnitude is about 6–10 W m^{-2} lower than ERA-Interim throughout the seasonal cycle. It is likely that ECCO has corrected the magnitude of the seasonal cycle in ERA-Interim. ECCO differs from OAFlux–CERES mostly during January–February, when ECCO Q_{net} is about 6–7 W m^{-2} lower than OAFlux–CERES in all basins. The rms values of the globally averaged seasonal cycles of Q_{net} from ECCO, OAFlux–CERES, ERA-Interim, and NCEP1 are 16.5, 16.8, 16.9, and 12.8 W m^{-2}, respectively.

The patterns of the seasonal cycles of the basinwide averaged Q_{net} differ with the basins (Figs. A2b–d), which may reflect the influence of the asymmetric distribution of the ocean basins between the Northern and Southern Hemispheres. For instance, the Indian Ocean is dominated by the ocean sector in the Southern Hemisphere, and the seasonal variation of Q_{net} is dictated by the season changes of the Southern Hemisphere (Fig. A2d), with an oceanic heat gain from September to March and a heat loss from April to September. In the Atlantic, the ocean area is roughly evenly distributed between the Southern and Northern Hemispheres, so the magnitude of the basin-averaged seasonal cycle is much smaller than those of the other ocean basins. The Q_{net} estimates differ most in the Atlantic Ocean (Fig. A2c). The three products, ECCO, OAFlux–CERES, and ERA-Interim, depict a similar semiannual cycle of Q_{net}, with a major maximum around September and a secondary maximum around April. By contrast, NCEP1 produces an annual cycle, with the seasonal maximum completely different from the other three. The subtropical regions in the Atlantic are responsible for the difference of NCEP1 from other products. In general, ECCO has the weakest seasonal Q_{net} in all basins. In the Atlantic, the ECCO Q_{net} is about 15–20 W m^{-2} weaker than ERA-Interim and about 5 W m^{-2} weaker than OAFlux–CERES.

REFERENCES

Booth, B. B. B., N. J. Dunstone, P. R. Halloran, T. Andrews, and N. Bellouin, 2012: Aerosols implicated as a prime driver of twentieth-century North Atlantic climate variability. *Nature*, **484**, 228–232, doi:10.1038/nature10946.

Bourassa, M. A., and Coauthors, 2013: High-latitude ocean and sea ice surface fluxes: Challenges for climate research. *Bull. Amer. Meteor. Soc.*, **94**, 403–423, doi:10.1175/BAMS-D-11-00244.1.

Bromwich, D. H., and R. L. Fogt, 2004: Strong trends in the skill of the ERA-40 and NCEP–NCAR reanalyses in the high and

midlatitudes of the Southern Hemisphere, 1958–2001. *J. Climate*, **17**, 4603–4619, doi:10.1175/3241.1.

Chen, X., and K.-K. Tung, 2014: Varying planetary heat sink led to global-warming slowdown and acceleration. *Science*, **345**, 897–903, doi:10.1126/science.1254937.

Chiodo, G., and L. Haimberger, 2010: Interannual changes in mass consistent energy budgets from ERA-Interim and satellite data. *J. Geophys. Res.*, **115**, D02112, doi:10.1029/2009JD012049.

Dee, D. P., and Coauthors, 2011: The ERA-Interim reanalysis: Configuration and performance of the data assimilation system. *Quart. J. Roy. Meteor. Soc.*, **137**, 553–597, doi:10.1002/qj.828.

Forget, G., J. M. Campin, P. Heimbach, C. Hill, R. M. Ponte, and C. Wunsch, 2015: ECCO version 4: An integrated framework for non-linear inverse modeling and global ocean state estimation. *Geosci. Model Dev.*, **8**, 3071–3104, doi:10.5194/gmdd-8-3653-2015.

Gulev, S. K., M. Latif, N. Keenlyside, W. Park, and K. P. Koltermann, 2013: North Atlantic Ocean control on surface heat flux on multidecadal timescales. *Nature*, **499**, 464–467, doi:10.1038/nature12268.

IPCC, 2013: *Climate Change 2013: The Physical Science Basis.* Cambridge University Press, 1535 pp.

Jin, X., L. Yu, D. L. Jackson, and G. A. Wick, 2015: An improved near-surface specific humidity and air temperature climatology for the SSM/I satellite period. *J. Atmos. Oceanic Technol.*, **32**, 412–433, doi:10.1175/JTECH-D-14-00080.1.

Josey, S. A., S. Gulev, and L. Yu, 2013: Exchanges through the ocean surface. *Ocean Circulation and Climate: A 21 Century Perspective*, G. Siedler et al., Eds., Academic Press, 115–140.

Kalnay, E., and Coauthors, 1996: The NCEP/NCAR 40-Year Reanalysis Project. *Bull. Amer. Meteor. Soc.*, **77**, 437–471, doi:10.1175/1520-0477(1996)077<0437:TNYRP>2.0.CO;2.

Karl, T. R., and Coauthors, 2015: Possible artifacts of data biases in the recent global surface warming hiatus. *Science*, **348**, 1469–1472, doi:10.1126/science.aaa5632.

Kato, S., N. G. Loeb, F. G. Rose, D. R. Doelling, D. A. Rutan, T. E. Caldwell, L. Yu, and R. A. Weller, 2013: Surface irradiances consistent with CERES-derived top-of-atmosphere shortwave and longwave irradiances. *J. Climate*, **26**, 2719–2740, doi:10.1175/JCLI-D-12-00436.1.

Large, W. G., and S. G. Yeager, 2004: Diurnal to decadal global forcing for ocean and sea-ice models: The data sets and flux climatologies. NCAR Tech. Note TN-460+STR, 105 pp., doi:10.5065/D6KK98Q6.

Levitus, S., J. I. Antonov, T. P. Boyer, R. A. Locarnini, H. E. Garcia, and A. V. Mishonov, 2009: Global ocean heat content 1955–2008 in light of recently revealed instrumentation problems. *Geophys. Res. Lett.*, **36**, L07608, doi:10.1029/2008GL037155.

Liang, X., C. Wunsch, P. Heimbach, and G. Forget, 2015: Vertical redistribution of oceanic heat content. *J. Climate*, **28**, 3821–3833, doi:10.1175/JCLI-D-14-00550.1.

Loeb, N. G., B. A. Wielicki, D. R. Doelling, G. L. Smith, D. F. Keyes, S. Kato, N. Manalo- Smith, and T. Wong, 2009: Toward optimal closure of the Earth's top-of-atmosphere radiation budget. *J. Climate*, **22**, 748–766, doi:10.1175/2008JCLI2637.1.

Mayer, M., K. E. Trenberth, L. Haimberger, and J. T. Fasullo, 2013: The response of tropical atmospheric energy budgets to ENSO. *J. Climate*, **26**, 4710–4724, doi:10.1175/JCLI-D-12-00681.1.

Meehl, G. A., J. M. Arblaster, J. T. Fasullo, A. Hu, and K. E. Trenberth, 2011: Model-based evidence of deep-ocean heat uptake during surface-temperature hiatus periods. *Nat. Climate Change*, **1**, 360–364, doi:10.1038/nclimate1229.

Solomon, S., J. S. Daniel, R. Neely, J.-P. Vernier, E. G. Dutton, and L. W. Thomason, 2011: The persistently variable background stratospheric aerosol layer and global climate change. *Science*, **333**, 866–870, doi:10.1126/science.1206027.

Stammer, D., K. Ueyoshi, A. Köhl, W. G. Large, S. A. Josey, and C. Wunsch, 2004: Estimating air–sea fluxes of heat, freshwater, and momentum through global ocean data assimilation. *J. Geophys. Res.*, **109**, C05023, doi:10.1029/2003JC002082.

Trenberth, K. E., J. T. Fasullo, and J. Kiehl, 2009: Earth's global energy budget. *Bull. Amer. Meteor. Soc.*, **90**, 311–323, doi:10.1175/2008BAMS2634.1.

Valdivieso, M., and Coauthors, 2016: An assessment of air–sea heat fluxes from ocean and coupled reanalyses. *Climate Dyn.*, doi:10.1007/s00382-015-2843-3, in press.

Wunsch, C., and P. Heimbach, 2013: Dynamically and kinematically consistent global ocean circulation and ice state estimates. *Ocean Circulation and Climate: A 21st Century Perspective*, G. Siedler et al., Eds., Academic Press, 553–579.

——, and ——, 2014: Bidecadal thermal changes in the abyssal ocean. *J. Phys. Oceanogr.*, **44**, 2013–2030, doi:10.1175/JPO-D-13-096.1.

Yu, L., and R. A. Weller, 2007: Objectively analyzed air–sea heat fluxes for the global ice-free oceans (1981–2005). *Bull. Amer. Meteor. Soc.*, **88**, 527–539, doi:10.1175/BAMS-88-4-527.

——, and X. Jin, 2014a: Confidence and sensitivity study of the OAFlux multisensor synthesis of the global ocean surface vector wind from 1987 onward. *J. Geophys. Res.*, **119**, 6842–6862, doi:10.1002/2014JC010194.

——, and ——, 2014b: Insights on the OAFlux ocean surface vector wind analysis merged from scatterometers and passive microwave radiometers (1987 onward). *J. Geophys. Res.*, **119**, 5244–5269, doi:10.1002/2013JC009648.

——, ——, and R. A. Weller, 2007: Annual, seasonal, and interannual variability of air–sea heat fluxes in the Indian Ocean. *J. Climate*, **20**, 3190–3209, doi:10.1175/JCLI4163.1.

——, ——, and ——, 2008: Multidecade global flux datasets from the Objectively Analyzed Air–Sea Fluxes (OAFlux) project: Latent and sensible heat fluxes, ocean evaporation, and related surface meteorological variables. OAFlux Project Tech. Rep. OA-2008-01, 64 pp.

——, and Coauthors, 2013: Towards achieving global closure of ocean heat and freshwater budgets: Recommendations for advancing research in air–sea fluxes through collaborative activities. WCRP Informal Series Rep. 13/2013, 42 pp.